Proc. of SPIE Vol. 3132, Optomechanical Design and Precision Instruments, ed. A E Hatheway (Oct 1997) Copyright SPIE

Using Finite Element Analysis and Fractography to Resolve a Flex Pivot Failure Problem*

Keith B. Doyle, Steven E. Forman
MIT Lincoln Laboratory
244 Wood St., Lexington, MA 02173-9108

ABSTRACT

As part of the Laboratory's Infrared Thermal Sounder (ITS) development program sponsored by NOAA, a Michelson Interferometer was designed and prototyped into hardware. The design included a moving mirror mechanism, which physically resembles a classical 4-bar linkage and utilizes two flex pivots at each of the four rotational joints. During the course of random vibration testing, to simulate spacecraft launch loads, pivots at one or both of the base locations of the linkage structurally failed. Finite element analysis showed that high stress concentrations existed at fillet locations on the pivot's internal flexures. Fractography analysis was used to determine that during manufacture crack generation sites formed at the fillet locations during stamping of the flexure blades. It was concluded that the flex pivots failed due to low-cycle fatigue at these locations. The solution was to limit the stress in the flexure blade using load shunts.

Keywords: flex pivot, fractography, finite element analysis, low-cycle fatigue, stress concentration, random vibration

1. INTRODUCTION

A flex pivot is a mechanical device which allows for the replacement of bearings in some rotating joints. A typical unit is illustrated in Figures 1a.-b. It consists of three flexures contained within two cylinders which are attached so that when one end of the device is held the other can undergo essentially frictionless torsional rotation. The flex pivots are usually made using 400 series stainless steels, and the flexures can be either brazed or welded into the cylinders. During normal use, these devices can maintain their performance through 10^8 to 10^9 torsional cycles. During random vibration testing, however, these types of flex pivots have had a previous record of failure (e.g., References 1, 2, 3) depending on the level of vibration. Usually the device employing flex pivots is caged or locked during vibration testing, and the pivots can be subjected to higher than allowable loads for short periods of time. For the most part, the failures have been blamed on the presence of defective welds or braze joints which had cracked during the tests. Instances of flexure buckling were also observed. Most problems were solved by either redesigning the flex pivot to have no welds (i.e., using an electric-discharge machined part), using larger diameter pivots or by using shunts to limit pivot radial movement. What seemed missing from all the descriptions of these failures was a fundamental understanding of how loads were transmitted through these devices and where high stress points might be located. The authors sought to gain that understanding and apply it to the failures that were occurring in the Laboratory's interferometer flex pivot joints.

2. CATALOG AND FACTORY VISIT INFORMATION

The flex pivots selected for use in the interferometer are nominally 6.35 mm (0.25 in.) in outer diameter. The maximum allowable load in the x-y plane according to the catalog [4] is 157 N (35.4 pounds). The flex pivot coordinate system is illustrated in Figure 2. During a factory visit, one of the authors observed that more than twice the catalog load could be applied statically before the onset of buckling or structural failure in either X or Y directions.

During the random vibration tests, the worst case 3-σ loads at the failed flex pivot locations were predicted (based on nearby accelerometer measurements and a finite element model of the interferometer) to be slightly greater than the catalog allowable. The failures which occurred during the vibration tests, however, bore no resemblance to those which were observed during the static loading tests.

* This work was sponsored by the National Oceanographic and Atmospheric Administration. Opinions, interpretations, conclusions, and recommendations are those of the author and are not necessarily endorsed by the National Oceanographic and Atmospheric Administration.

During the factory visit, staff identified the materials in the flexures and cylinders as 420 stainless steel (Rockwell C Hardness = 46) and 410 stainless steel, respectively.

The Metals Handbook [5] lists the following properties for the flexure material which is considered to be ductile:

Ultimate Strength = 1.59 GPa (230 ksi)
Yield Strength = 1.34 Gpa (195 ksi)
Endurance Limit = 0.76 Gpa (110 ksi)

The cylinders are machined parts and the flexures are stamped. Based on their experience, the manufacturer staff recommended for their parts that an endurance limit of 0.41 Gpa (60 ksi) be used rather than the higher handbook value.

Based on these properties and prior to using the flex pivots, one needs to determine an allowable stress range for dynamic loading situations and how induced stresses throughout the pivot correlate to the applied loads. In order to probe this area, finite element models were created of 6.35 and 7.94 mm (1/4 and 5/16-inch) flex pivots, loads were applied in various directions and stresses were predicted. This modeling is described in the next section.

3. FLEX PIVOT FINITE ELEMENT MODELING AND RESULTS

MSC/NASTRAN finite element models of 6.35-mm and 7.94-mm (1/4-inch and 5/16-inch) diameter flex pivots were developed. A model is shown in Figure 3. The models were used to determine the stiffness of the pivots and the load-stress distribution within the individual flexure blades. The loads applied to the flex pivot during vibration testing were extrapolated from nearby accelerometers and a finite element model of the interferometer assembly [8] which utilized the stiffness values generated from the flex pivot model.

The transverse stiffness values were computed using a guided top end boundary condition and a fixed base (this best represented the flex pivot mounted in the interferometer assembly). A unit transverse force was then applied at the center location of the top outer sleeve in eight different orientations. An example is illustrated in Figure 4. The four axes are denoted by the letters Y, C, P, and X. The stiffness in each of the axes is directional dependent which is denoted for the Y, C, and P axes by a subscript, c, for compression and, t, for tension. The X axis direction is denoted with, r, for right and, l, for left. (Refer to Figure 2). The eight transverse load cases were used to determine the best flex pivot orientation within the interferometer assembly by the orientation which produced the least pivot load. The rotational and axial stiffness of the flex pivot was computed by holding the top sleeve and applying a unit moment and unit axial force, respectively.

The finite element model of the interferometer assembly was used to generate the loads carried by the flex pivots under the launch environment. Uncoupled spring elements using the average spring constant obtained for each axis from the flex pivot model were used in the interferometer model to account for the stiffness of the flex pivot. This allowed a practical and efficient approach to estimate the flex pivot loads via the interferometer model, and, at the same time, to use the detailed flex pivot model to understand the blade stresses.

The first step taken to determine the stress levels in the blades was to impose unit loads on the flex pivot model. These loads were applied in both directions of the X and Y-axes for a total of four load cases. For unit loads applied in the X and Y-directions, the maximum stress is 42 Mpa and 46 Mpa (6.1 ksi and 6.7 ksi), respectively, for the 6.35-mm (1/4-inch) flex pivot. For the 7.94-mm (5/16-inch) flex pivots, the maximum stresses for the unit loads are 31 Mpa (4.5 ksi) for the X-axis and 28 Mpa (4.1 ksi) for the Y-axis. The critical stresses occur at the fillets of the inboard top and bottom flexure blades as shown in Figures 5.

The next step was to scale the results based on the 3-σ random force levels from the interferometer model based on a linear elastic analysis. The forces generated by the interferometer assembly model for the 6.35-mm (1/4-inch) flex pivot in the X and Y-axis were 179 N and 119 N (40.2 lbs and 26.7 lbs), respectively, during the random vibration spectrum test. These forces produce stresses at the fillet in the flexure blades which exceed the yield stress of the material. A non-linear analysis would be required to understand the redistribution of the state of stress past yield.

In summary, the primary conclusion to be drawn from the finite element modeling was that the flex pivots were being loaded dynamically beyond their yield limit many times over the duration of the random vibration test. Forces in the X-Y plane were causing these excessive stresses at the inboard fillets of the free ends of the two outside flexures.

4. FRACTOGRAPHY OF FAILED SURFACES

As described in the previous section, the finite element model indicated that the flex pivots were being overstressed at certain flexure fillets during random vibration testing. The authors postulated that cracks initiated at stamping defect sites in the fillets, propagated toward the weld lines, and either stopped or progressed along the welds to the other side of the flexures. Once the end fixities of the flexures were changed, they were subject to buckling at lower than normal values.

Figure 6 is an example of one of the failed flex pivots where the free end was completely separated from the flexure blade. The corner marked "failure initiation site" is at an inboard free end fillet. A closer examination using a scanning electron microscope is illustrated in Figure 7 and indicates four nearly parallel striations spaced about 0.03 mm (0.001 inches) apart. These markings indicate that a crack likely initiated in the lower right hand corner during dynamic overstress, and then propagated in an "orderly" manner and proceeded through "fast fracture," and then the crack became long enough so that "material tearing" occurred. The tearing was sufficiently ductile to peen over the edges of the crack surface as it proceeded to the other edge of the flexure blade. In speaking to various materials and fracture surface experts [6], the physical appearance of the failure surface was identified as a classic example of crack propagation during low cycle, ductile fatigue.

There were also flex pivots where the failure was not as dramatic. Working carefully with a high power microscope, an inboard free-end fillet with a crack was photographed as shown in Figure 8. The crack appears as a white scratch against the dark background. The crack appears to have initiated at an overstressed defect site and propagated to the weld line at the center of the flexure where it terminated. A similar crack was found in the same place in the other outboard flexure of the flex pivot, exactly as predicted by the finite element modelling. Subsequent viewing of 10 failed flex pivots indicated damage which was consistent with this type of failure theory.

In light of a better understanding of the flex pivot failure mode, some flex pivots which were thought to have survived random vibration tests were revisited microscopically. In two instances, barely visible cracks were observed at the suspect fillets of the outboard flexure blades.

5. SELECTING AN ALLOWABLE DESIGN STRESS

In reviewing the loads applied to the flex pivots which had failed random vibration tests and to those which had passed, the following correlations to stress levels in the fillets could be made from finite element modelling:

1. Some failures occurred where predicted 3-σ stresses were as low as 1.0 GPa (150 ksi).

2. No failures occurred where predicted 3-σ stresses were 0.6 GPa (90 ksi) or below.

In light of these observations, an appropriate maximum allowable 3-σ design stress for random vibration was set at 0.69 GPa (100 ksi). This stress level corresponds to an applied load of 66 to 76 N (15 to 17 pounds) for the X-Y plane of the 6.35 mm (1/4-inch) flex pivot. (Note for the 7.94-mm (5/16-inch) pivot, 98 to 111 N (22 to 25 pounds) produces 0.69 Gpa (100 ksi) at the fillets). It is interesting to note that this value range is about half that listed in the catalog and that this magnitude of reduction was initially suggested to us by researchers at JPL for dynamic loading [3].

6. EFFECTS OF WELD QUALITY AND FACTORY SCREENING

In viewing the failed flex pivots, particular attention was paid to the weld joints. There was no evidence that weld failures caused any flexure failures in the lots used for the Laboratory interferometer. The load path through the flexure blades does not appear to couple with apparent stress concentrations caused by unwelded areas at the flexure-free end interface to the inner cylinder.

The blade passes between two barrel parts and is welded from the outside inward. With a 0.30 mm (0.012-inch) wall thickness the weld penetrates 0.13 to 0.25-mm (0.005 to 0.010 inch) leaving as much as 0.18-mm (0.007-inch) unwelded. The rationale behind this geometry is to keep the weld heat from weakening the blade properties where it meets the barrel. It is not comforting, however, that as much as 50% of the joint can go unwelded.

Another area of concern was the method the manufacturer used to screen flex pivots prior to delivery. Each 6.35-mm flex pivot (1/4 inch) was loaded statically to 222 N (50 pounds) in the X-Y plane at the factory. Finite element analyses show that this loading causes plastic yield at the inboard free end fillets of the outer flexure blades. Fortunately, since the material is ductile, the stress redistributes itself, and cracks do not occur. We could find no evidence of cracks in any statically loaded parts, even those loaded to failure. In searching the literature, there is no evidence that this type of screening load has any effect on the ultimate low cycle fatigue strength, in cases where applied dynamic loads exceed yield [7]. Once again, however, it is not comforting that these devices were loaded beyond yield prior to delivery.

7. REVISITING THE INTERFEROMETER DESIGN

Once a failure theory and reasonable design criteria were in hand, an attempt was made to modify the interferometer to reduce flex pivot loads. A lighter motor was selected to lessen the 3-σ in-plane loads applied to pivot locations which had previously failed. However, these changes still did not bring the fillet stresses down to 0.69 Gpa (100 ksi) at the desired launch load levels. The finite element model of the 7.94-mm (5/16-inch) pivot described earlier was exercised, however, the stress levels still remained excessive at the desired launch loads.

Load shunts were designed to limit the radial travel of the flex pivots to displacements which corresponded to a maximum fillet stress of 0.69 Gpa (100 ksi). Based on the finite element model, a radial clearance of about 0.03-mm (0.0012-inch) corresponds to a predicted stress of 0.69 Gpa (100 ksi). During subsequent random vibration testing, the shunted pivots survived the desired launch levels illustrated in Figure 8 and are currently being implemented into the interferometer design.

8. CONCLUSIONS

In summary, the flex pivot failures which occurred during random vibration testing of the Laboratory built Michelson interferometer were caused by a low-cycle fatigue of overstressed flexure fillet defect sites. The use of stamped flexure blades provided crack generation sites which coupled with loads which exceeded allowable values. In future efforts, these blades should be chemically etched prior to insertion in the flex pivots in order to eliminate the defect sites.

Determination of allowable stresses to use during random vibration testing required a high fidelity finite element model of a flex pivot to be developed and exercised. This model was used to generate load-stress profiles for each of the degrees of freedom of a flex pivot. A maximum, 3-σ design stress of 0.69 Gpa (100 ksi) was thought to be reasonable and for the 6.35-mm (1/4-inch) flex pivot in question, corresponded to reducing the catalog allowable load by a factory of slightly more than two.

In the case of the interferometer, the design was too far advanced to permit major changes. Load shunts were employed to limit radial pivot excursions so that failure stresses could not be achieved in the flexure blades during the desired random vibration sequence and subsequent testing has been successful. In conclusion, resolution of the flex pivot failure problem was accomplished by coupling high fidelity finite element modelling with microscopic fractography to better understand the operation of the flex pivots and to establish realistic guidelines for their use.

ACKNOWLEDGMENTS

The authors are grateful to their colleagues: A. Colao, R. Purdy, D. Bold and J. Ingwerson of Lincoln Laboratory for their help along the way. Appreciation is also given to T. Mower, P. Daniels, and W. DiNatale of Lincoln Laboratory and Dr. Peter Hilton, a private consultant from Concord, Massachusetts, for their assistance in interpreting and photographing failure surfaces.

REFERENCES

1. Stark, K.W., and Wilson, M., "A Mirror Transport Mechanism for Use at Cryogenic Temperatures," N87-16327.

2. Williams, E.I., Summers, R.T., and Ostaszewski, M.A. "High Performance Reactionless Scan Mechanism," N95-27288.

3. Private Communication with D. Juergens at Jet Propulsion Laboratory, February 1996.

4. Lucas Aerospace, Free Flex-Pivot Frictionless Bearing Catalog, Publication Number 00U-6-901D.

5. "Metals Handbook, 8th Edition, Volume 12, Properties and Selection of Metals," American Society for Metals, 1961.

6. Private Communications with T. Mower of Lincoln Laboratory and P. Hilton of Concord, Mass.

7. Werchniak, W., "Effect of Pre-Stress on Low Cycle Fatigue," Engineering Fracture Mechanics, Volume 4, Dec. 1992, p 841-851.

8. The Interferometer Computer Model was developed by J. Ingwerson of Lincoln Laboratory.

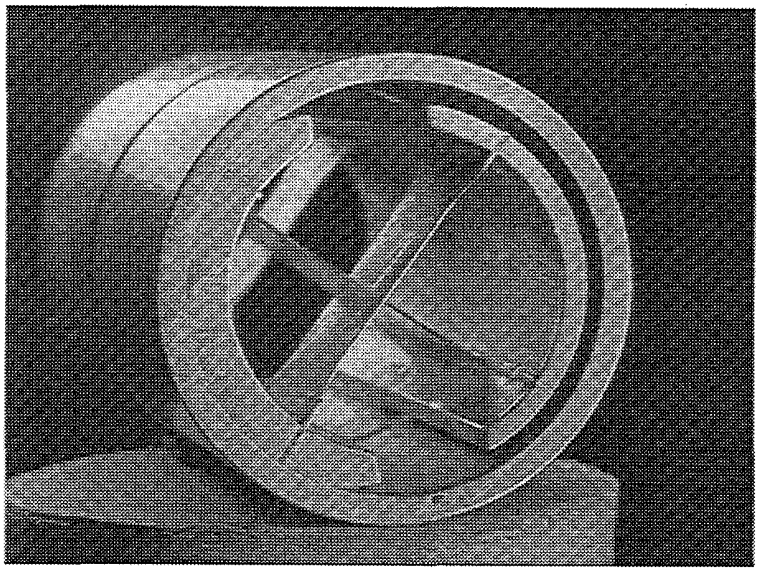

Figure 1a. Typical Flex Pivot

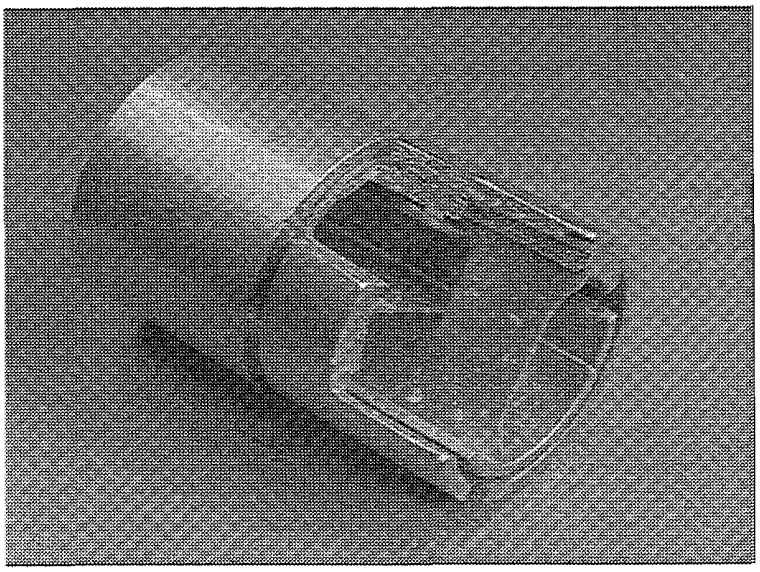

Figure 1b. Cut-away View Of Flex Pivot

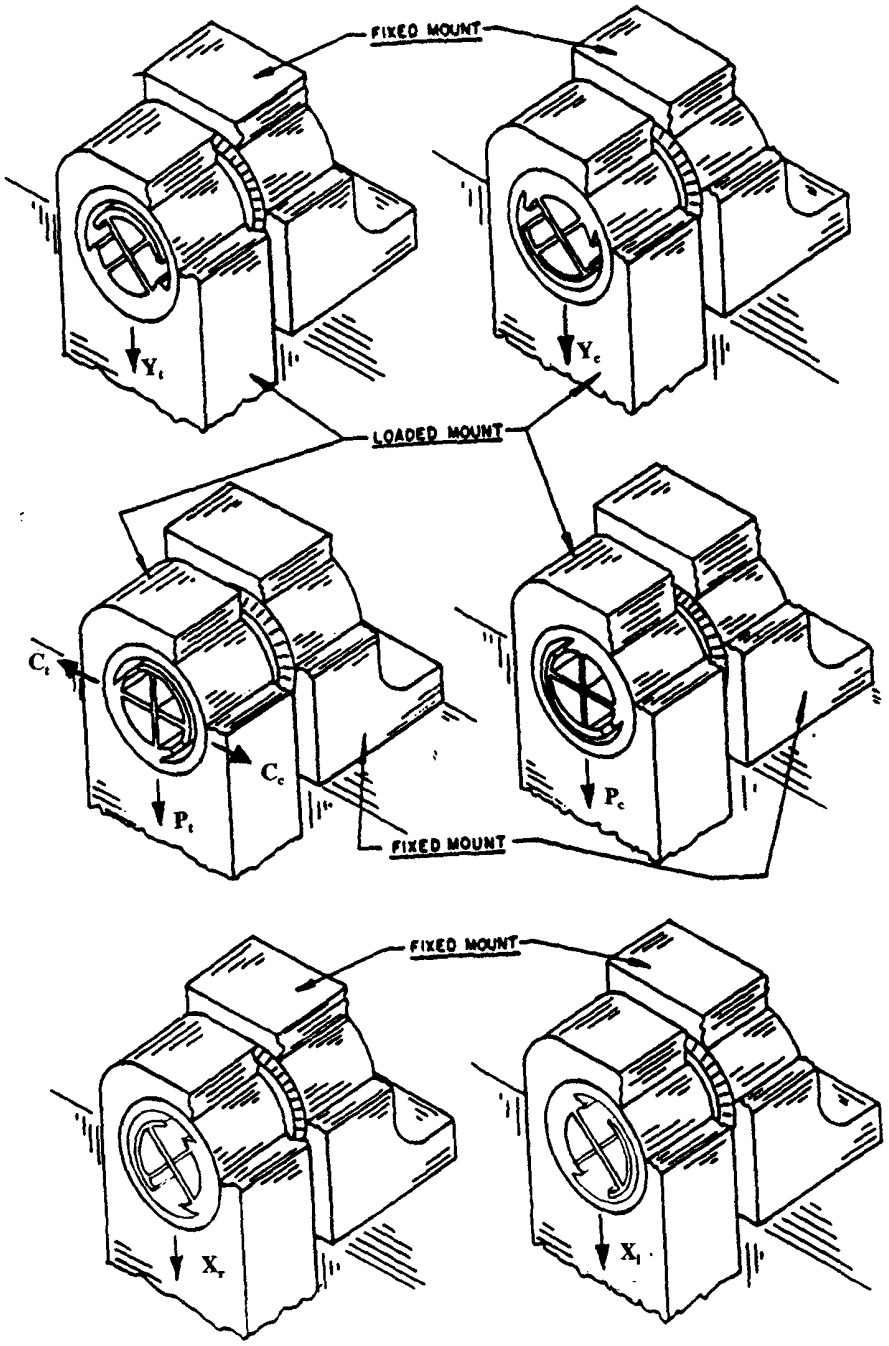

Figure 2. Flex Pivot Coordinate System

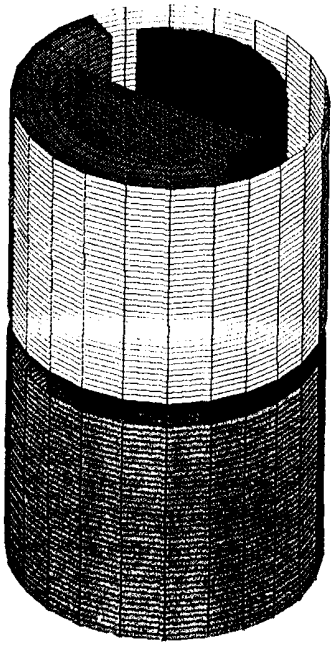

Figure 3. Flex Pivot Finite Element Model

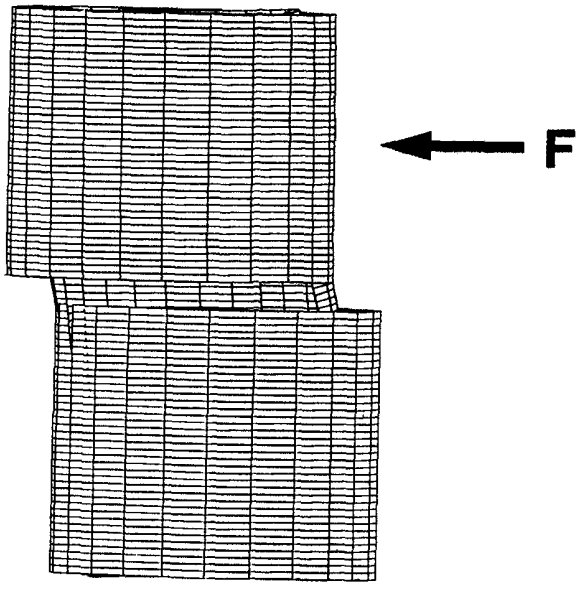

Figure 4. Transverse Load Condition

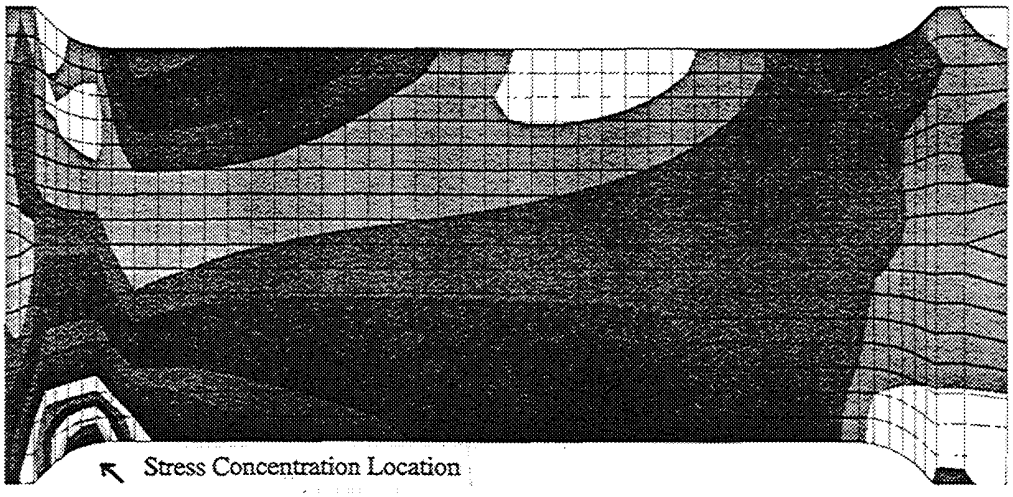

Figure 5. Finite Element Stress Plot of Flex Pivot Blade

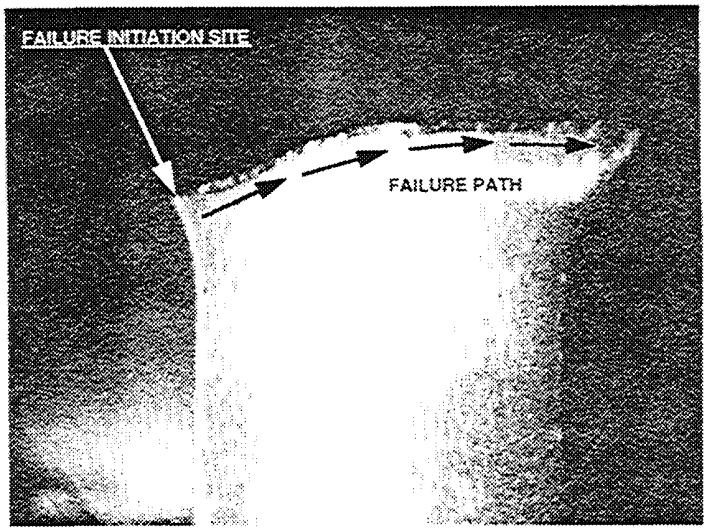

Figure 6. Failed Flex Pivot Blade

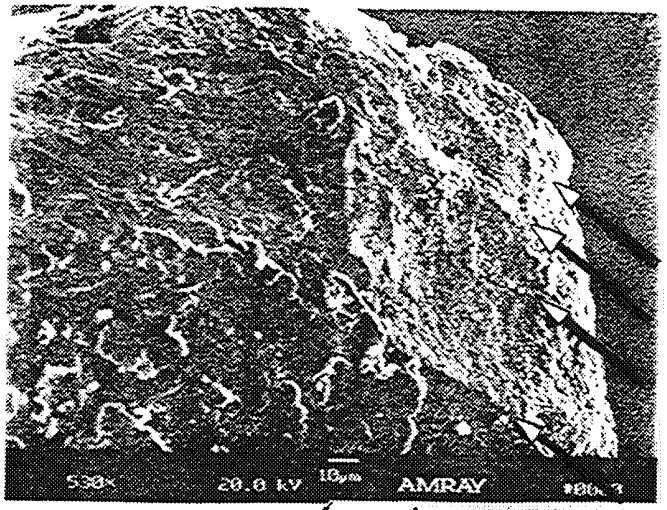

(arrows denote parallel striations)

Figure 7. Failure Surface

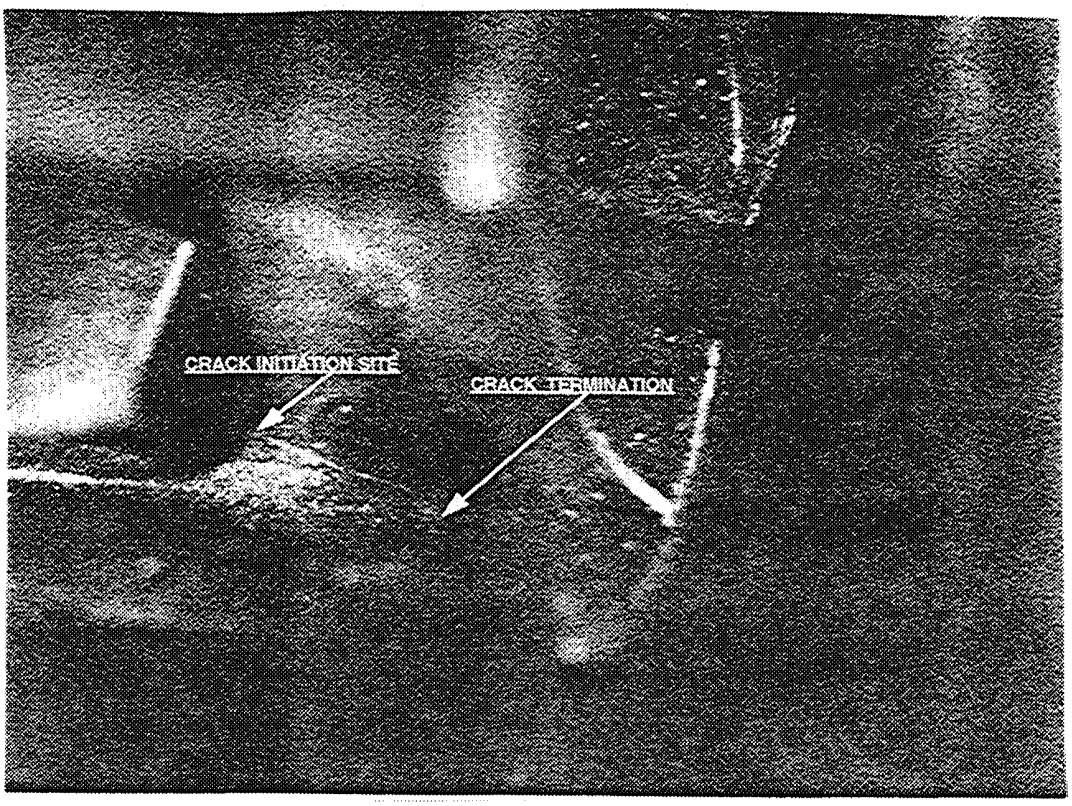

Figure 8. Flex Pivot Blade Crack